It does occur in the actual setup by two distinct paths. The external static electric field can mix $2S_{1/2}$ and $2P_{1/2}$, thus allowing an $E1$ transition from $2S_{1/2}$ to $2P_{1/2}$ by the microwave field. This path involves no parity violation. Alternatively, the $2S_{1/2}$–$2P_{1/2}$ mixing can occur through H_{PV}, followed by the same $E1$ transition. The transition rate involves an interference between these two paths, and takes the form[24], for the specific conditions of the Michigan experiment,

$$R = R_0[1 \pm 2.5 \times 10^{-6} C_{2P}]$$

where R_0 is the rate in the absence of H_{PV}. The $\pm$ sign occurs for different relative orientations of the various electric and magnetic fields. Therefore, if C_{2P} is a number of order 1, as suggested by equation (2), the transition rate will vary by about 1 p.p.m. as the fields are reversed. The experimenters believe that they can detect this small variation in a reasonable amount of running time. Similar experiments are being carried out at Yale University and at the University of Washington. In each case it is expected that the experiments can be done in deuterium as well as hydrogen. The Yale experiment will be sensitive to a different combination of C_1 and C_2. The successful completion of these experiments will then give the values of each of the four constants that determine H_{PV}.

If further calculations and experiments in heavy atoms and in H and D confirm the Bi results, it will be necessary to modify the theory leading to equations (1) and (2). A number of proposals along this line already exist[25,26]. Some of these new models predict that C_{1P}, C_{1N} both vanish, but C_{2P}, C_{2N} do not[25]. These models lead to greatly decreased effects in heavy atoms but results similar to the standard model in H and D. In other models all four of the C_i are very small or zero[26], and therefore predict diminished parity violation effects everywhere. The H and D experiments will obviously be very useful in distinguishing between these models. Some results are expected within the next year.

This research was supported in part by the US Department of Energy.

1. Mislow, K. *Introduction to Stereochemistry* (Benjamin, New York, 1966).
2. Letokhov, V. S. *Phys. Lett.* 53A, 275 (1975).
3. Townes, C. & Schawlow, A. *Microwave Spectroscopy* (McGraw Hill, New York, 1955).
4. Bernstein, J. *Elementary Particles and their Currents* (W. H. Freeman, San Francisco, 1968).
5. Sandars, P. G. H. in *Atomic Physics IV* (ed. Putlitz, Zu. *et al.*) (Plenum, New York, 1975).
6. Weinberg, S. *Phys. Rev. Lett.* 19, 1264 (1967).
7. Salam, A. in *Elementary Particle Physics* (ed. Svantholm, N.) (Almquist & Wicksells, Stockholm, 1968).
8. Holder, M. *et al. Phys. Lett.* 72B, 254 (1977).
9. Feinberg, G. & Chen, M. Y. *Phys. Rev.* D10, 3789 (1974).
10. Bouchiat, M. A. & Bouchiat, C. *J. Phys.* 35, 899 (1974).
11. Bouchiat, M. A. & Pottier, L. *J. Phys. Lett.* 36L, 189 (1977).
12. Chu, S. *et al. Phys. Lett.* 60A, 96 (1977).
13. Baird, P. E. G. *et al. Nature* 264, 528 (1976).
14. Lewis, L. L. *et al. Phys. Rev. Lett.* 39, 795 (1977).
15. Baird, P. E. G. *et al. Phys. Rev. Lett.* 39, 798 (1977).
16. Novikov, V. *et al. Soviet Physics, JETP* 44, 872 (1976).
17. Henley, E. M. & Wilets, L. *Phys. Rev. A.* 14, 1411 (1976).
18. Brimicombe, M. W. S. M. *et al. J. Phys.* B9, L237 (1976).
19. Sternheimer, R. *Phys. Rev.* 84, 244 (1951).
20. Henley, E. M. *et al. Phys. Rev. Lett.* 39, 994 (1977).
21. Loving, C. E. & Sandars, P. G. E. (19) preprint.
22. Lewis, R. R. & Williams, W. L. *Phys. Lett.* 59B, 70 (1970).
23. Azimov, Ya. *et al. Soviet Physics, JETP* 40, 8 (1975).
24. Dunford, R. W. *et al. Phys. Rev. A.* (in the press).
25. Zee, M. A. B. & Zee, A. *Phys. Rev. Lett.* 30, 675 (1973).
26. Mohapatra, R. N. & Sidhu, D. P. *Phys. Lett.* 38, 667 (1977).

articles

Silicalite, a new hydrophobic crystalline silica molecular sieve

E. M. Flanigen, J. M. Bennett, R. W. Grose, J. P. Cohen, R. L. Patton & R. M. Kirchner

Union Carbide Corporation, Tarrytown Technical Center, Tarrytown, New York 10591

J. V. Smith

Department of Geophysical Sciences, University of Chicago, Chicago, Illinois 60637

A new polymorph of SiO_2 (silicalite, refractive index 1.39, density 1.76 g cm^{-3}) has a novel topologic type of tetrahedral framework. This encloses a three-dimensional system of intersecting channels defined by 10-rings wide enough to adsorb molecules up to 0.6 nm diameter. Silicalite is hydrophobic and organophilic, and selectively adsorbs organic molecules over water.

A MAJOR scientific and technological achievement since 1949 has been the discovery and development of synthetic crystalline, aluminosilicate zeolites as molecular sieve adsorbents and catalysts. We now report the synthesis, crystal structure, and properties of silicalite, a new microporous crystalline silica with remarkable sieve properties. Unlike aluminosilicate zeolites which are hydrophilic, silicalite is hydrophobic and organophilic, and selectively adsorbs organic molecules in the presence of water.

The crystal structure is a new topologic type of tetrahedral framework, which contains a large fraction of five-membered rings of silicon–oxygen tetrahedra. The framework outlines a three-dimensional system of intersecting channels defined by 10-rings of oxygen ions in all three directions. Organic quaternary ammonium ions which occupy the channels in the precursor obtained by hydrothermal synthesis, are removed by heating to yield silicalite. The resulting void occupies about 33% of the crystal volume, and the three-dimensional channel is wide enough to adsorb molecules up to about 6 Å in diameter. Silicalite can be heated to near 1,300 °C where it degrades to a glass.

Synthesis

The silicalite precursor is crystallised hydrothermally in a closed system containing alkylammonium cations (for example, tetrapropylammonium), hydroxyl ions, and a reactive form of silica at 100–200 °C. The organic-containing precursor crystals have a typical empirical composition $(TPA)_2O \cdot 48SiO_2 \cdot H_2O$, mean refractive index 1.48, and measured density 1.99 g cm^{-3}. The organic cation is larger than the pore and therefore must be removed by chemical or thermal decomposition (usually calcination in air at 500–600 °C) to yield the microporous silicalite

crystals (mean refractive index 1.39, d[illegible]y 1.76 g cm^{-3}). As the silica framework is electrically neutral, the organic ion is apparently occluded with hydroxyl ions to maintain charge balance, as indicated by infrared spectroscopy. The unit cell composition for the precursor crystals can be expressed as [4TPAOH·96SiO_2] Unlike aluminium-containing zeolites, silicalite has no cation exchange properties.

The crystallisation mechanism of the precursor seems to involve silica clathration of the hydrophobic organic cation analogous to the formation of crystalline water clathrates of alkylammonium salts[1-3]. Thus the silica tetrahedra assemble into a framework in place of the hydrogen-bonded water 'lattice' of the water clathrate, and surround the hydrophobic organic guest molecules. The alkylammonium ion seems to enhance the solubility of silica in water in a manner reminiscent of the 'structure-breaking' or 'cluster' forming properties of these same ions in aqueous solution[3]. Indeed, the alkylammonium ion further links the chemistry and structure of water and silica, and seems to translate the structural chemistry of water below room temperature to silica near 200 °C.

Crystal structure

Precursor crystals are typically 20×20×70 μm elongated along *c*, and commonly occur as interpenetrant twins on the (110) plane. Crystals calcined to 600 °C over 2 d have unit-cell edges *a*, 20.06; *b*, 19.80; *c*, 13.36 Å. The systematic absences (*hk*0, $h = 2n+1$; 0*k*1, $k+1 = 2n+1$) indicate space group Pnma or Pn2$_1$a. Although the symmetry is apparently orthorhombic, weak diffractions may result from either lower symmetry or intergrowth of a second phase. From 8,297 diffraction intensities collected with monochromatised CuKα radiation out to 2θ 110° with a Picker FACS-I diffractometer, 3,542 unique diffractions were obtained with 764 above background (3σ). The crystal was twinned, and overlap of diffractions was corrected for the 90 : 10 ratio of the twin volumes.

Combination of direct methods (MULTAN program) and model building yielded the structure in Pn2$_1$a (Table 1). The 96 tetrahedra per unit cell form a 4-connected framework with a system of intersecting channels (Fig. 1) composed of near-circular zig-zag channels along *a* (free cross-section 5.4±0.2 Å) cross-linked by elliptical, straight channels along *b* (free cross-section 5.7–5.8×5.1–5.2 Å). Both channels are defined by 10-rings. The calculated free cross-section assumes that oxygen ions have a radius of 1.3 Å, and depends slightly on the choice of diametrically-opposing oxygens. The channel system same topology as that reported for a 'shape-selective' has the zeolite[4], but structural details were not given.

Figure 2*A* is a photograph down the *b* axis of a model constructed from tetrahedral stars and plastic linkages. Figure 3*A* is a topological drawing showing how the framework can be constructed from pairs of tetrahedra, 4-rings and corrugated bands of 6-rings all cross-linked by 5-rings and occasional 6-rings. Figure 3*B* shows the *a*-axis projection. The corrugated bands of 6-rings are seen end-on, and each 4-ring lies between

Fig. 1 Idealised channel system in silicalite. To avoid possible confusion caused by the perspective, the dimensions of the channels along *c* are shown at upper centre.

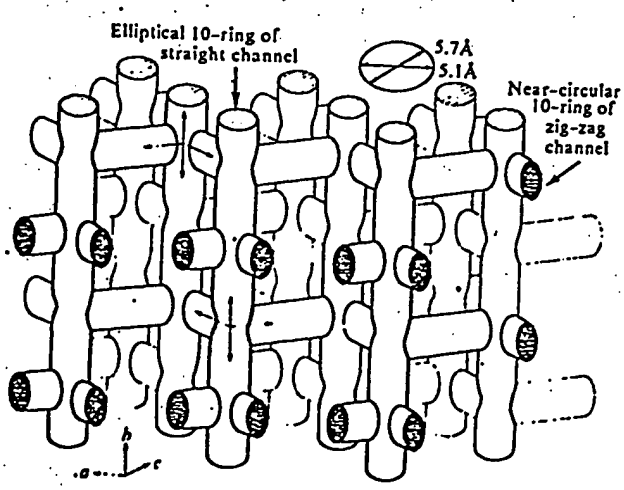

Table 1 Atom positions in silicalite

Atom	*x*	*y*	*z*
SI (1)	0.4225 (6)	0.5468 (3)	0.3518 (9)
SI (2)	0.3055 (9)	0.5150 (10)	0.1944 (7)
SI (3)	0.1902 (2)	0.5570 (2)	0.3197 (6)
SI (4)	0.0687 (7)	0.5225 (8)	0.1616 (9)
SI (5)	0.2160 (8)	0.4223 (8)	0.4595 (10)
SI (6)	0.3752 (8)	0.4401 (10)	0.4627 (10)
SI (7)	0.0788 (8)	0.3597 (10)	0.1744 (10)
SI (8)	0.1888 (10)	0.3056 (10)	0.3060 (10)
SI (9)	0.3166 (10)	0.3582 (10)	0.1586 (10)
SI (10)	0.4266 (9)	0.3193 (10)	0.3227 (10)
SI (11)	0.1220 (10)	0.3138 (11)	0.9710 (10)
SI (12)	0.0754 (7)	0.1208 (8)	0.1912 (10)
SI (13)	0.1965 (9)	0.1517 (8)	0.3032 (10)
SI (14)	0.3187 (10)	0.1150 (10)	0.1766 (12)
SI (15)	0.4228 (10)	0.1631 (10)	0.3005 (12)
SI (16)	0.1184 (9)	0.1586 (10)	0.9320 (11)
SI (17)	0.2727 (8)	0.3166 (9)	0.9773 (11)
SI (18)	0.2752 (7)	0.1658 (9)	0.9599 (11)
SI (19)	0.2267 (9)	0.0492 (10)	0.4464 (11)
SI (20)	0.3845 (9)	0.0592 (8)	0.4818 (11)
SI (21)	0.4249 (8)	0.9393 (10)	0.3132 (12)
SI (22)	0.3063 (9)	0.9575 (10)	0.1701 (11)
SI (23)	0.1881 (9)	0.9450 (10)	0.3239 (12)
SI (24)	0.0590 (8)	0.9051 (8)	0.1989 (10)
O (1)	0.3834 (16)	0.3370 (17)	0.2262 (21)
O (2)	0.3730 (17)	0.5271 (18)	0.2454 (22)
O (3)	0.4837 (18)	0.5483 (17)	0.2972 (23)
O (4)	0.2409 (17)	0.5344 (18)	0.2262 (22)
O (5)	0.3047 (18)	0.4414 (19)	0.1849 (23)
O (6)	0.1082 (19)	0.5474 (18)	0.2573 (22)
O (7)	0.1234 (18)	0.3419 (19)	0.2806 (23)
O (8)	0.2527 (17)	0.3213 (18)	0.2209 (24)
O (9)	0.2995 (18)	0.3313 (17)	0.0822 (23)
O (10)	0.0963 (19)	0.3102 (18)	0.0572 (23)
O (11)	0.1306 (17)	0.1508 (19)	0.2555 (24)
O (12)	0.4967 (16)	0.1527 (17)	0.2721 (22)
O (13)	0.3214 (17)	0.0614 (18)	0.1352 (23)
O (14)	0.3687 (17)	0.1690 (18)	0.2261 (24)
O (15)	0.2481 (18)	0.1473 (16)	0.2212 (23)
O (16)	0.3214 (16)	0.1481 (18)	0.0394 (22)
O (17)	0.0836 (16)	0.4454 (19)	0.1702 (24)
O (18)	0.9931 (18)	0.3393 (18)	0.1904 (25)
O (19)	0.4274 (17)	0.2462 (19)	0.3529 (20)
O (20)	0.3866 (16)	0.4978 (18)	0.4116 (25)
O (21)	0.1827 (17)	0.4747 (18)	0.3853 (22)
O (22)	0.4039 (19)	0.3795 (18)	0.4059 (25)
O (23)	0.1907 (18)	0.3629 (18)	0.4021 (24)
O (24)	0.2892 (16)	0.4112 (17)	0.4760 (20)
O (25)	0.1802 (16)	0.4479 (18)	0.5685 (20)
O (26)	0.4021 (17)	0.4694 (16)	0.5966 (21)
O (27)	0.1974 (18)	0.2503 (18)	0.3459 (20)
O (28)	0.2054 (16)	0.3315 (16)	0.9469 (18)
O (29)	0.0696 (15)	0.3590 (16)	0.9334 (20)
O (30)	0.1011 (12)	0.2550 (16)	0.9533 (20)
O (31)	0.2768 (16)	0.2320 (18)	0.9137 (19)
O (32)	0.0818 (17)	0.1548 (17)	0.0798 (19)
O (33)	0.0766 (18)	0.0362 (18)	0.1714 (22)
O (34)	0.2074 (16)	0.1165 (18)	0.4281 (20)
O (35)	0.3970 (16)	0.1289 (16)	0.3892 (21)
O (36)	0.1917 (17)	0.1492 (17)	0.9844 (20)
O (37)	0.0959 (17)	0.1096 (16)	0.8882 (22)
O (38)	0.2978 (18)	0.3715 (17)	0.8828 (23)
O (39)	0.3030 (19)	0.1275 (16)	0.8621 (20)
O (40)	0.1989 (18)	0.0438 (17)	0.5593 (19)
O (41)	0.4144 (18)	0.0564 (17)	0.5818 (22)
O (42)	0.3853 (17)	0.9245 (18)	0.2291 (19)
O (43)	0.2588 (16)	0.9544 (18)	0.2675 (19)
O (44)	0.1171 (16)	0.9156 (17)	0.2414 (19)
O (45)	0.5020 (16)	0.9461 (17)	0.2986 (22)
O (46)	0.3103 (17)	0.0342 (16)	0.4894 (19)
O (47)	0.4198 (16)	0.9896 (17)	0.3833 (22)
O (48)	0.1992 (18)	0.9823 (17)	0.4196 (21)

Values in parentheses following the values for the atom parameters are the error values. The temperature factor was fixed at 1.0 for the silicon atoms and 2.5 for the oxygen atoms.

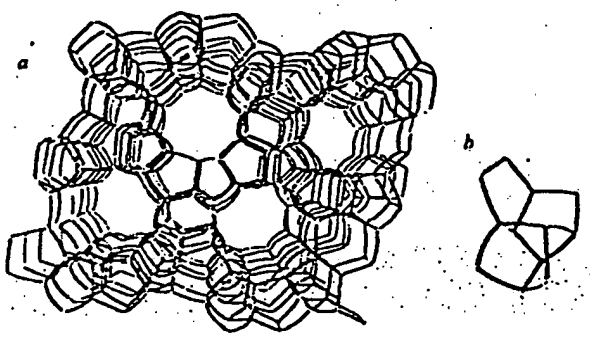

Fig. 2 *A*, Framework viewed down *b*: *B*, Secondary building unit of structure. Twelve tetrahedra linked into five 5-rings and one 6-ring.

two linked pairs. Particularly interesting is the high percentage of 5-rings, a feature shared with the zeolites dachiardite, mordenite, ferrierite and epistilbite. Two other polymorphs of silica, coesite and melanophlogite, also contain 5-rings. The frameworks of the zeolites listed above contain an infinite sheet of linked 6-rings, which might be regarded as a subunit involved in synthesis[5,6]. Perhaps the corrugated bands of 6-rings may be regarded as a sub-unit in the synthesis of silicalite. Alternatively, the silicalite structure can be assembled from subunits of 12 linked tetrahedra (Fig. 2*B*).

The structural subunits of silicalite can be assembled into other structure types, as will be described elsewhere. These theoretical frameworks give calculated X-ray powder patterns which do not match the observed X-ray powder pattern for silicalite. The present structure gives a calculated pattern which fits well with the observed pattern (Fig. 4). Because of the weakness of intensities from the small crystal used for the structure determination, the *R* factor is rather high at 0.16. The twinning of silicalite around {110} may be due to faulting perpendicular to *b* allowing a pseudo-tetragonal framework that permits *a* and *b* axes to interchange giving the appearance of a (110) twin axis. An 'hourglass' zoning is also seen on the (010) and (100) faces. The calculated density is 1.80 g cm^{-3} in good agreement with the measured 1.76 g cm^{-3}.

Fig. 3 Topologic drawings of silicalite structure. *A*, *b*-axis projection, *B*, *a*-axis projection. Si atoms lie at the intersections of the lines, and O atoms approximately half-way along the lines. Triple bands of corrugated 6-rings are shown by thick and thin continuous lines. Pairs of tetrahedra and 4-rings occur in projection in (*B*) as dots and circles and as linked open and filled triangles. In (*A*) the pairs of tetrahedra and the 4-rings superimpose as linked dots of two sizes. The corners of the unit cell are shown, together with screw diad axes of symmetry.

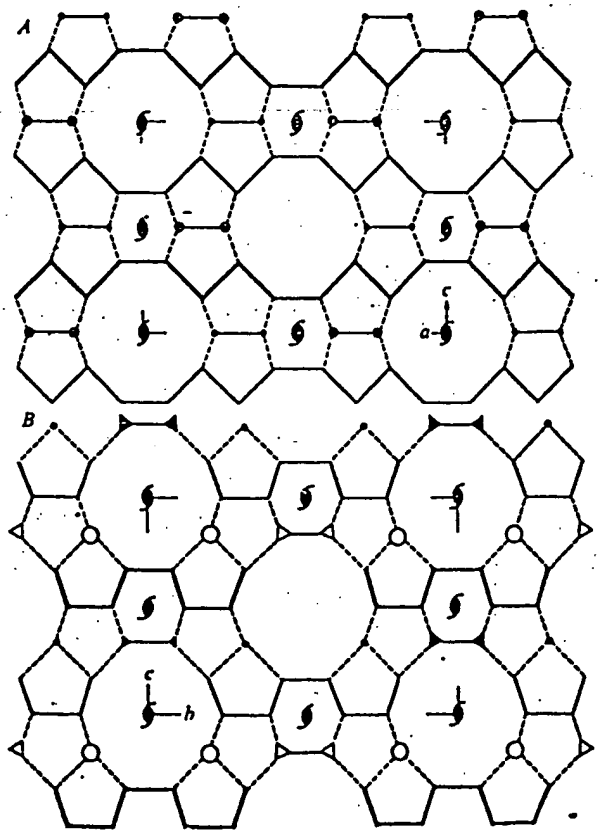

Adsorption

Silicalite is a molecular sieve adsorbent with an adsorption pore size near 6 Å and a saturation adsorption pore volume of 0.19 cm^3 g^{-1} in agreement with the properties expected from its crystal structure. At ambient temperature, it adsorbs molecules as large as benzene (kinetic diameter 5.85 Å) but rejects molecules larger than 6 Å, such as neopentane (kinetic diameter 6.2 Å). Although the pore-size effect can be used in molecular sieving, its most remarkable adsorption property is surface selectivity. In contrast to the extremely high preference of aluminosilicate zeolite surfaces for water (hydrophilic) and other polar molecules, silicalite has a very low selectivity for the adsorption of water and a very high preference for the adsorption of organic molecules smaller than its limiting pore size. This hydrophobic and organophilic selectivity manifests itself in several ways. Adsorption of organic molecules and permanent gases on silicalite occurs by the volume filling of micropores as in zeolite molecular sieves and other microporous adsorbents. The filling of micropores occurs by physical adsorption at low relative pressures, and is characterised by enhancement of the adsorption energy due to increase of dispersion forces resulting from comparable size of the adsorption volume and the adsorbed molecule. This results in a type I, near rectilinear isotherm as illustrated for the gas phase adsorption of *n*-hexane on silicalite (Fig. 5*b*). Pore filling is essentially complete at a relative pressure of 0.03. In contrast, water does not fill the pores at any relative pressure (Fig. 5*a*). The adsorbed water volume at a relative pressure near one is about 25% of the saturation pore volume for *n*-hexane. In liquid or gaseous mixtures of organic molecules and water, silicalite selectively adsorbs the organic molecule, and thus is capable of removing organic molecules from organic–water streams.

Most solid surfaces are hydrophilic. Previously known hydrophobic surfaces[7] include graphitised carbon and microporous and macroporous silicas which have been rendered hydrophobic by removal of the hydrophilic surface hydroxyl groups either by thermal dehydration and dehydroxylation or by chemical modification of the surface to replace the hydroxyl

Table 2 Adsorption volumes in silicalite

Adsorbate	Temperature (° C)	Kinetic diameter (Å)	V_p (cm^3 g^{-1})	V_t	Molecules adsorbed per unit cell
H_2O	RT	2.65	0.047	0.083	15.1
O_2	−183	3.46	0.185	0.326	38.0
CH_3OH	RT	3.8	0.193	0.340	27.6
n-Butane	RT	4.3	0.190	0.334	10.9
n-Hexane	RT	4.3	0.199	0.350	8.8
SF_6	RT	5.5	0.167*	—	10.9
C_6H_6	RT	5.85	0.134	0.236	8.7
Neo-pentane	RT	6.2	0.029	0.051	1.4

V_p (cm^3 g^{-1}) = Total micropore volume in activated silicalite from saturation capacity, calculated using normal liquid densities at the adsorption temperature. Void fraction, $V_t = V_p$ (cm^3 g^{-1}) × d_c (g cm^{-3}), where d_c is the measured density 1.76 g cm^{-3}. All samples activated by calcination in air at 600 °C followed by vacuum activation (10^{-3} torr). Adsorption measurements all by gravimetric McBain-Bakr balance technique. RT, room temperature.
*At 760 torr.

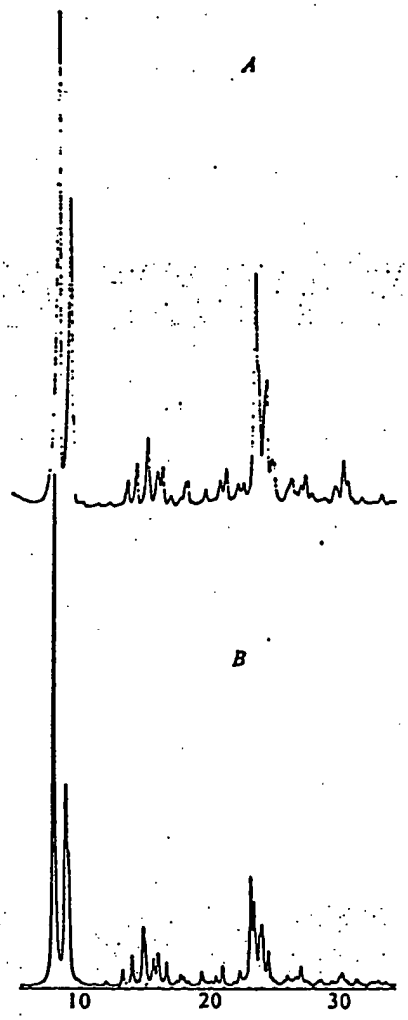

Fig. 4 X-ray powder diffraction pattern of *A*, calcined silicalite material, and *B*, calculated from parameters in Table 1. CuKα radiation with scale in degrees 2θ.

groups with hydrophobic organic or organosiloxane groups. The water isotherms (Fig. 5*A*) for Graphon, a dehydrated 'HiSil' silica, and a carbon molecular sieve with a pore size (5.0–5.5 Å) and pore volume (0.20 $cm^3 g^{-1}$) comparable to that of silicalite, suggest that the silicalite surface is similar to or more hydrophobic than the Graphon and dehydrated HiSil surface. The carbon molecular sieve (commercial Pittsburgh activated carbon, Calgon Type MSC-V) is more hydrophilic.

The nature of a hydrophobic adsorbent surface has become understood within the last decade and is reviewed comprehensively in ref. 7. For physical adsorption on an ionic surface, the adsorption interaction energy consists of the sum of dispersion and repulsion energies which originate from non-specific interactions, and electrostatic polarisation, dipole and quadrupole energies which represent specific interactions. For adsorption of water, specific interactions are especially important. In the absence of surface sites which are 'hydrophilic', or of sites for hydrogen bonding, polar or acid–base interactions, the surface becomes nonspecific, homogeneous and hydrophobic. In water, each molecule is hydrogen-bonded to its neighbours (approximately four, as in ice), but in silicalite the narrowness of the channels allows interaction with only about two to three molecules on the average. Because silicalite is electrically neutral, there is no strong interacti n with water molecules, and energetically the molecules prefer to remain as a liquid outside the silicalite. What small amount is adsorbed in silicalite is probably associated with the residual hydroxyl groups which persist after thermal removal of the organic ion in the precursor. The initial isosteric heat of adsorption of water on silicalite is about 6 kcal mol^{-1}, substantially below that of the heat of liquefacti n of water (9.7 kcal mol^{-1}), and similar t that reported for Graphon[7]. This requires a high entropy of adsorption, again lik Graphon. Low energy and high entropy of adsorption (weak adsorption f highly entropic water) indicate high mobility of the adsorbed water molecule. The strongly hydrophilic nature of aluminosilicate zeolite molecular sieves is due to the presence in the intracrystalline void space of polar groups such as cations and hydroxyl groups, and field gradients generated by the substitution of aluminium for silicon in the tetrahedral framework. Silicalite has no aluminium and no cations in its structure. Chen[8] has shown a substantial decrease in the amount of water adsorbed on the zeolite mordenite (Zeolon) due to the removal of cations, as well as aluminium from the aluminosilicate framework,

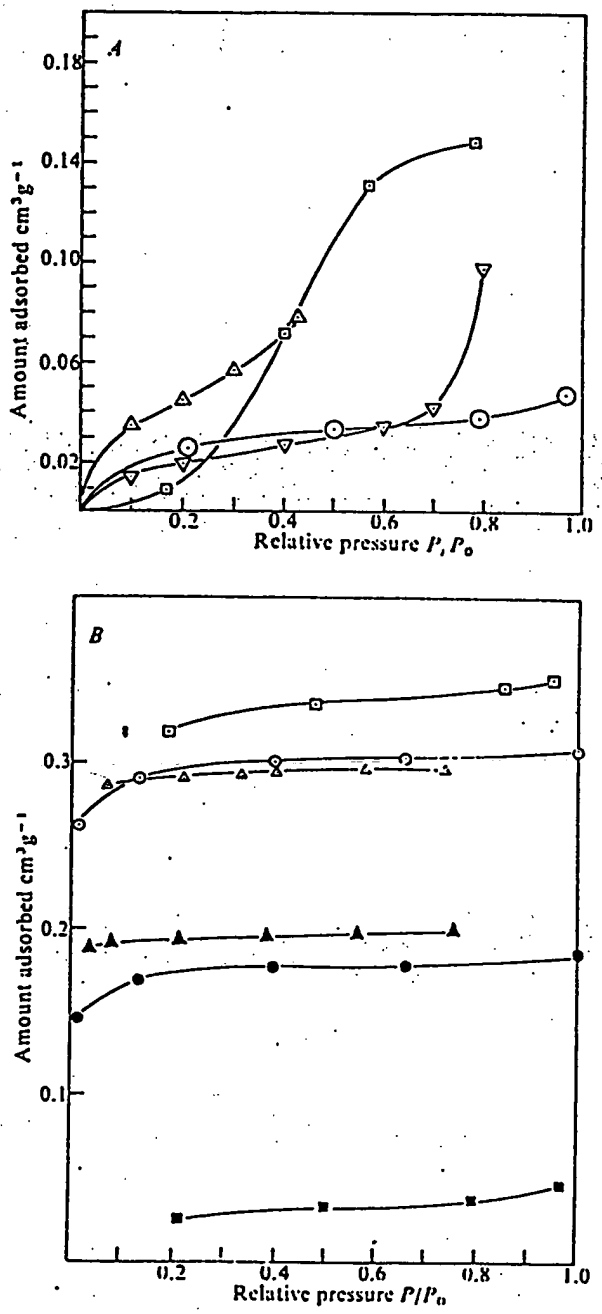

Fig. 5 *A* Water adsorption isotherms on hydrophobic surfaces. □, Carbon molecular sieve; △, Graphon; ▽, Hi Sil; ○, silicalite. *B*, Adsorption isotherms on silicalite and NaX zeolite. O_2 at −183 °C, samples activated at 350 °C, 10^{-3} torr; McBain–Bakr gravimetric measurements. □, H_2O on NaX; ○, O_2 n NaX; △, *n*-hexane n NaX; ▲, *n*-hexane on silicalite; , O_2 on silicalite; ■, H_2O on silicalite.

and described the resulting highly siliceous zeolites as 'hydroph bic'.

Adsorption of *n*-hexane in contrast is highly energetic with isosteric heats of adsorption of 16–18 kcal mol^{-1} ver a wide range of relative pressure. This range is substantially above the heat of liquefaction of *n*-hexane (7.8 kcal mol^{-1}), and similar to the isosteric heat of adsorption of *n*-hexane on the molecular sieve zeolite X, again illustrating the high dispersion energy interactions in crystalline molecular sieves where the adsorption cavities and pores are ≤ 10 Å, commensurate with the size of the adsorbed molecule. Consideration of the volume, size and geometry of the void in the silicalite structure (Figs 1–3) and the number and size of *n*-hexane molecules (8.8 molecules per unit cell and 4.5 Å kinetic diameter) shows that the molecules must be highly oriented in nearly linear strings one molecule thick. The fit of *n*-hexane in the channels is near perfect, and *n*-hexane becomes a low entropy highly ordered liquid in the silicalite lattice. Typical adsorption volumes for a variety of molecules on silicalite are given in Table 2.

Stability

Silicalite possesses a remarkable stability for a 33% porous crystal. It is stable in air to over 1,100 °C, and only slowly c nverts to an amorphous glass at 1,300 °C. It is stable to most mineral acids but reacts with HF similarly to quartz. X-ray emission measurements of the SiKβ band show that the mean Si–O bond energy of silicalite exceeds that of quartz by 0.1 eV, and is essentially the same as for cristobalite. In contrast, the mean Si–O bond energy in aluminosilicate zeolites is substantially less than for quartz[9].

Applications

Thus silicalite may offer practical applications in the clean-up of water contaminated with organic compounds. Traces of methanol, propanol, butanol, phenol, 1,4-dioxane, pentane and hexane have been removed from water. The selectivity of silicalite is nearest to that of adsorbent carbons, but it has the advantage of much higher stability to regenerative commercial processes involving thermal, acid, and oxidative conditions.

We thank T. R. Cannan for his assistance in synthesis and adsorption characterisation, and Union Carbide Corporation for permission to publish this article.

Received 18 November; accepted 30 December 1977.

1. McMullan, R. K., Bonamico, M. & Jeffrey, G. A. *J. phys. Chem.* 39, 3295 (1963).
2. Barrer, R. M. *Adv. Chem. Ser.* 121, 1–28 (1973).
3. Perron, G., Desrosiers, N. & Desnoyers, J. E. *Can. J. Chem.* 54, 2163 (1976).
4. Meisel, S. L., McCullough, J. P., Lechthaler, C. H. & Weisz, P. B. *Chemtech*, Feb., 86 (1976).
5. Merlino, S. *Soc. Italiano di Mineralogia e Petrologia—Rendiconti* 31, 513–540 (1975).
6. Meier, W. M. in *Natural Zeolites: Occurrence, Properties and Use* (eds Sand, L. B. & Mumpton, F. A.) (Pergamon, Elmsford, New York, in the press).
7. Zettlemoyer, A. C. in *Hydrophobic Surfaces* (ed. Fowkes, F. M.) 13–24 (Academic, New York, 1969).
8. Chen, N. Y. *J. phys. Chem.* 80, 60–64 (1976).
9. Patton, R. L., Flanigen, E. M., Dowell, L. G. & Passoja, D. E. *ACS Symp. Ser.* 40, 64–75 (1977).

Radon emanation on San Andreas Fault

Chi-Yu King

U S Geological Survey, 345 Middlefield Road, Menlo Park, California 94025

Subsurface radon emanation monitored in shallow dry holes along an active segment of the San Andreas fault in central California shows spatially coherent large temporal variations that seem to be correlated with local seismicity.

RADON is constantly emanated from the Earth into its atmosphere normally in minute amounts. Radon emanation is known to be anomalously large on active faults and to show temporal variations related to changing atmospheric conditions and possibly nearby seismic activities[1,2]. To check whether it may show premonitory changes useful for earthquake prediction like those reported for the emanation from deep aquifers[3,4], the US Geological Survey began on 7 May 1975 to monitor subsurface radon emanation in 20 shallow dry holes along an active 60-km segment of the San Andreas and Calaveras faults in central California (stations 1-20, Fig. 1). Here I present some initial results of this experiment and discuss possible explanations.

We used a simple track etch method[5–7] that had been developed for uranium exploration to measure radon emanation: a small piece of plastic film (cellulose nitrate) which is sensitive to α radiation is attached to the inside bottom of a plastic cup (9 cm high, 7 cm aperture). The cup is placed upside down at the bottom of a borehole (10 cm in diameter, 0.7 m deep) to expose the film to the soil gas for 1 week, after which it is replaced by a new cup. The air gap in the cup is sufficient to shield the film from all α particles generated in the soil. As radon and its isotopes are gaseous, however, they may move into the cup to emit α particles close enough to leave tracks in the film. The retrieved film is then chemically etched and the enlarged α-particle tracks in the film within an area of nearly 6 mm^2 are counted under a microscope. The measured track density is then assumed to be proportional to the average radon

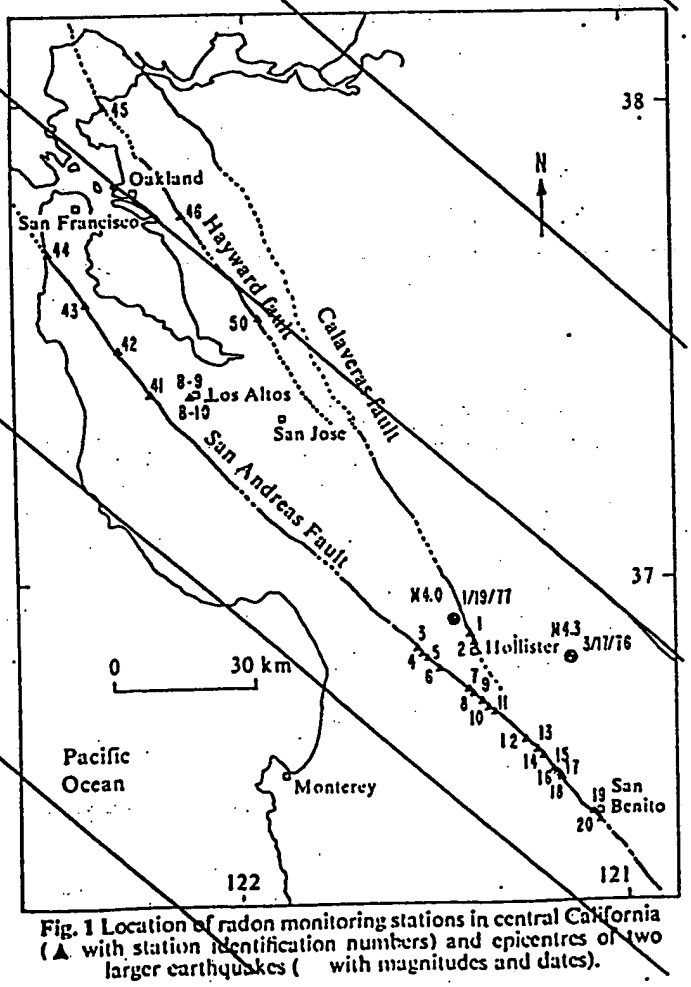

Fig. 1 Location of radon monitoring stations in central California (▲ with station identification numbers) and epicentres of two larger earthquakes (with magnitudes and dates).